Materials Research. 2023; 26:e20220339
DOI: https://doi.org/10.1590/1980-5373-MR-2022-0339

Effects of Argon Partial Pressure Variations on Wettability and Anti-icing Characteristics of Aluminum Doped ZnO Thin Films

***Nicky P. Patel*[a]*, Kamlesh V. Chauhan*[a]**

[a]*CHAMOS Matrusanstha Department of Mechanical Engineering, Chandubhai S. Patel Institute of Technology (CSPIT), Charotar University of Science and Technology (CHARUSAT), Changa, 388421, Gujarat, India.*

Received: July 29, 2022; Revised: December 27, 2022; Accepted: January 9, 2023

When ice forms on solid surfaces, it can cause issues in many different sectors (aircraft, electricity lines, etc.). Surfaces and coatings with hydrophobic qualities may be used in anti-icing applications. The purpose of this work is to utilize RF Magneton Sputtering to deposit AZO thin coatings, which will slow the accumulation of ice on the surface. The effects of changes in argon partial pressure on the anti-icing, wettability, optical, and structural properties of the resulting thin films have been experimentally investigated. X-ray diffraction demonstrated a (002) peak of ZnO, the intensity of the peak diminishes with an increase in partial pressure. The band gap was measured to be between 2.98 and 3.15 eV, and the average maximum transmittance was observed to be around 82% for 50% partial pressure and 71% for 33% partial pressure, confirming the transparency of the thin films. Wettability studies revealed that the films are hydrophobic with a maximum contact angle of 127.5°, which was deposited at lower partial pressure. Films deposited at 33% partial pressure delayed the formation of ice on the surface by 4.5 folds when compared to an uncoated substrate.

Keywords: *Sputtering, Al-doped Zinc Oxide (AZO), Wettability, Transmittance, Anti-icing, Hydrophobicity.*

1. Introduction

The development of ice on surfaces poses a significant risk to wind turbines, electrical transmission lines, passenger jets, and other structures[1-4]. Blackouts have been common in recent years due to ice-related catastrophes in electrical networks, such as tower collapse and conductor galloping. Traditional procedures used to get rid of ice like mechanical, electrical, and thermal are often inefficient, energy-wasting, and even damage the equipment[5]. Therefore, the investigation into efficient de-icing strategies was essential. Surfaces that imitate the non-stickiness along with the hydrophobic property of lotus leaves have drawn interest in both basic research and practical applications, such as anti-icing, self-cleaning, resistance to corrosion, separation of water and oil, waterproofing, and reduction in drag[6-10]. The two most crucial components in the accomplishment of such surfaces are the modification of the surface energy to be low, and the surface to be rough[11]. Due to economic values and high demand given by a broad range of applications of coating technologies, there has been a significant effort and energy put into the design and study of functional thin films and technologies[12]. Magnetron sputtering[13], sol-gel spin coating[14], atomic layer deposition[15], chemical vapor deposition[16], sol-gel dip coating[17], and pulsed laser deposition[18] are just a few of the techniques that can be employed to develop coatings.

Over the past few years, the n-type, group II-VI semiconductor aluminium doped zinc oxide (AZO) has received a lot of interest as a more environmentally friendly and less toxic substitute for the more widely used transparent conducting oxide indium tin oxide (ITO)[19]. There are numerous technologies and applications where ZnO can be employed as TCO, such as LED's, nonlinear optics, and thin film transistors, but most notably in the photovoltaic industry, by doping it with aluminum, high optical transmittance and electrical resistivity of 10^{-4} Ω.cm can be achieved. In terms of structure, AZO displays a hexagonal wurtzite crystal structure where Al^{3+} donors take the place of Zn^{2+} ions in the zinc oxide lattice. As a result, there are a lot more free electrons available for conduction, increasing the carrier concentration to somewhere between 4 to $11x10^{20}$ cm^{-3}. The optical properties of AZO include an average visual transmission of more than 80% and a broad direct band gap of at least 3.3 eV[20].

There seems to be little literature about the wettability and anti-icing of aluminium doped zinc oxide films, hence this is a topic of interest. It was worthwhile to assess the effect of surface structure on AZO surfaces as a function of varying argon partial pressure because the relationship between surface structure and anti-icing properties is not well understood. Here, RF magnetron sputtering using inert gases such as helium and argon was used to produce AZO thin films on a glass substrate. With slight variations in microstructure roughness, AZO hydrophobic surfaces were produced by adjusting the sputtering conditions (argon partial pressure). The anti-icing property of the surfaces was evaluated at -15 °C. Additionally, the effect of microstructure on the hydrophobic film's capacity to prevent icing was

*e-mail: nicky_ptl@yahoo.co.in

researched. According to this research, the coexistence of rough nanostructures and low-surface-energy elements is essential for producing properties that are both icephobic and hydrophobic.

2. Material and Methods

Al-doped ZnO target (ZnO/Al, 98/2 w%) of 50 mm diameter and 5 mm thickness was used to prepare thin films in a custom-made 16" diameter x 14" cylindrical vacuum chamber (Excel instruments, India) on glass substrate using a RF magnetron sputtering. The partial pressure of argon was varied from 33 to 50% which was controlled and measured using mass flow controller procured from Alicat, USA. The deposition time, working pressure, sputtering power and deposition temperature were 60 min., 2.5 Pa, 250 W, and 350 °C respectively. The parameters for the coatings are summarized in Table 1.

Utilizing a Bruker D2 phaser and Cu-Kα radiation with a wavelength of 1.54 Å, an X-Ray Diffractometer (XRD) was used to examine the structural attributes of the thin films that were formed. To analyse the morphology of the coatings, backscattered electrons of FESEM (Emitech, Evo-18) were utilised. In order to study the surface topography, an atomic force microscope (Bruker, Multimode Nanoscope-IV) was used and the scanning area was 5µm * 5µm. A Shimadzu 3600 spectrophotometer was used to evaluate the optical characteristics of Al-doped ZnO coatings. The wettability properties of the thin films were investigated using the sessile drop technique and a contact angle goniometer (Rame Hart 290). The icing conditions of the deposited thin films was investigated using a Peltier device at a temperature of -15 °C. Using thermal paste, the samples were attached directly to the Peltier cooler for uniform cooling.

3. Results and Discussion

The XRD results for the deposited thin films at 33, 38, 43, 47, and 50% argon partial pressure are shown in Figure 1. When the argon partial pressure reached 50%, a very low (002) peak of ZnO was observed; however, as the argon partial pressure was dropped to 47, 43, and 38%, the (002) peak of ZnO became more visible and its intensity increased significantly. The films deposited at 33% partial pressure displayed the highest peak, indicating that the thin films deposited at this pressure have the best crystallite structure among the others. The film is most likely being bombarded by energetic gas atoms as a result of ion neutralisation and reflection on the target surface. When the gas flow decreases, the atom's mean free path expands, resulting in additional bombardment. This may result in proper growth of the films and an increase in grain size.

The decrease in intensity of the (002) peak with an increase in gas flow rate from 40 sccm to 60 sccm was observed by Wu et al.[21], they also discovered that the microstructure was not much affected due to variations in gas flow rate. Similarly, a maximum intensity of (002) peak was observed at 0.3 Pa which gradually decreased with increase in the argon gas flow rate[22]. Shain et al.[23] observed (002) peak of ZnO when deposited AZO thin films by changing argon pressure from 10 to 30 sccm, moreover, they noticed that there was no impurity of aluminium seen in XRD patterns, and with the rise in argon pressure, the intensity of the peak diminished. The increase in the intensity of the (002) peak with the decrease in the argon partial pressure were also observed by other researchers[24-26].

Scherrer's Equation 1 was used to determine the average grain size of the prepared thin films[27]:

$$D = \frac{0.94\lambda}{\Delta\omega cos\theta_B} \quad (1)$$

where, D is the crystallite size, λ is the wavelength, θ_B is Bragg angle and Δω is peak's full width and half maximum.

It was observed from the calculation that as the argon content was reduced from 50% to 33%, the average crystallite size ascended from 10.87 nm to 24.22 nm. The average crystallite size of the coatings prepared at varied partial pressure is shown in Figure 2. Wu et al.[21] reported that the grain size declined with increasing gas flow, the highest grain size was 33.72 nm, recorded at 40 sccm, and that it decreased to 18 sccm for a flow rate of 60 sccm argon flow rate. The decrease in grain size from 28.85 to 23.43 nm with the rise in argon flow rate from 10 to 30 sccm was also observed by Shain et al.[23]. A similar increase in grain size of thin films from 6.3 to 14.8 nm with a decrease in argon flow rate was also observed by Wang et al.[28].

The impact of various argon partial pressure on AZO thin film surface morphology is shown in Figure 3. The surface of the coatings varied considerably as the argon partial pressure

Table 1. Sputtering conditions for preparing AZO thin films.

Target	AZO
Substrate	Corning glass
Substrate temperature	350 °C
Power	250 W
Base pressure	1 x 10^{-3} Pa
Sputtering Pressure	2.5 Pa
Target-substrate distance	50 mm
Inert Gas Partial Pressure (Ar:He)	33, 38, 43, 47 and 50%
Deposition time	60 minutes

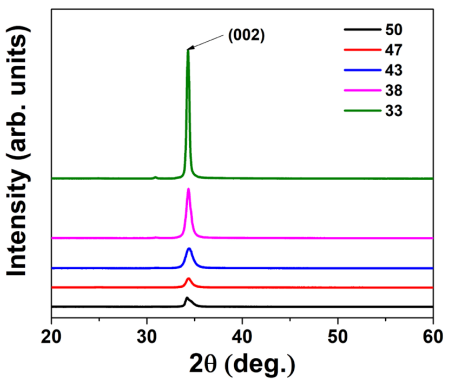

Figure 1. XRD spectra of AZO coatings prepared at different argon partial pressures.

was altered. The size of the grains and microstructure of the coatings prepared at lower partial pressure were found to be denser and coarser, whereas grain size decreases proportionally with increasing Ar flow rate. A low growth rate prevents the construction of a voided and uneven structure. This explanation for growth rate variation and its link with the mean free route of the species arriving at the developing surface is also supported by the surface morphology observed and in the structural analysis studied using XRD.

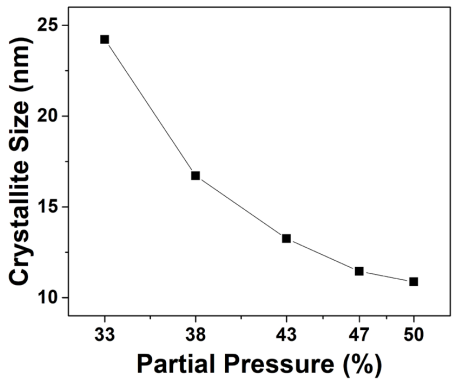

Figure 2. Average Crystallite Size of AZO coatings prepared at different argon partial pressures.

Figure 4 illustrates the topography of the zinc oxide films doped with aluminium. In comparison to thin films synthesized at lower partial pressure, those deposited at higher partial pressure were smooth. The coatings had a maximum roughness of 703 nm when deposited at 33%, 467 nm when coated at 43%, and a minimum roughness of 224 nm when deposited at 50%. When the partial pressure was increased, it was noticed that the roughness of the coating diminishes. The sputtered species lose energy due to frequent collisions and decreased mean free path, which in turn encourages self-shadowing as the partial pressure increases. As a result, increasing argon partial pressure causes the roughness to diminish[29]. According to a research by Han and Kim[24], the roughness decreased from 0.43 nm to 0.38 nm as the argon gas flow rate was elevated from 25 to 100 sccm. They reported that the coating roughness was affected by the argon flow rate and the grain size.

AZO thin films generated at varied argon partial pressure have their optical transmittance illustrated in Figure 5. The average transmittance of thin films developed at 33% partial pressure was 71%, while the average transmittance of thin films developed at 50% partial pressure was 82%, which indicates that the films became more transparent as the partial pressure was elevated.

In their research on the effects of argon pressure, Wang et al.[28] found that the films that were deposited were transparent and had a maximum value of 85%, which

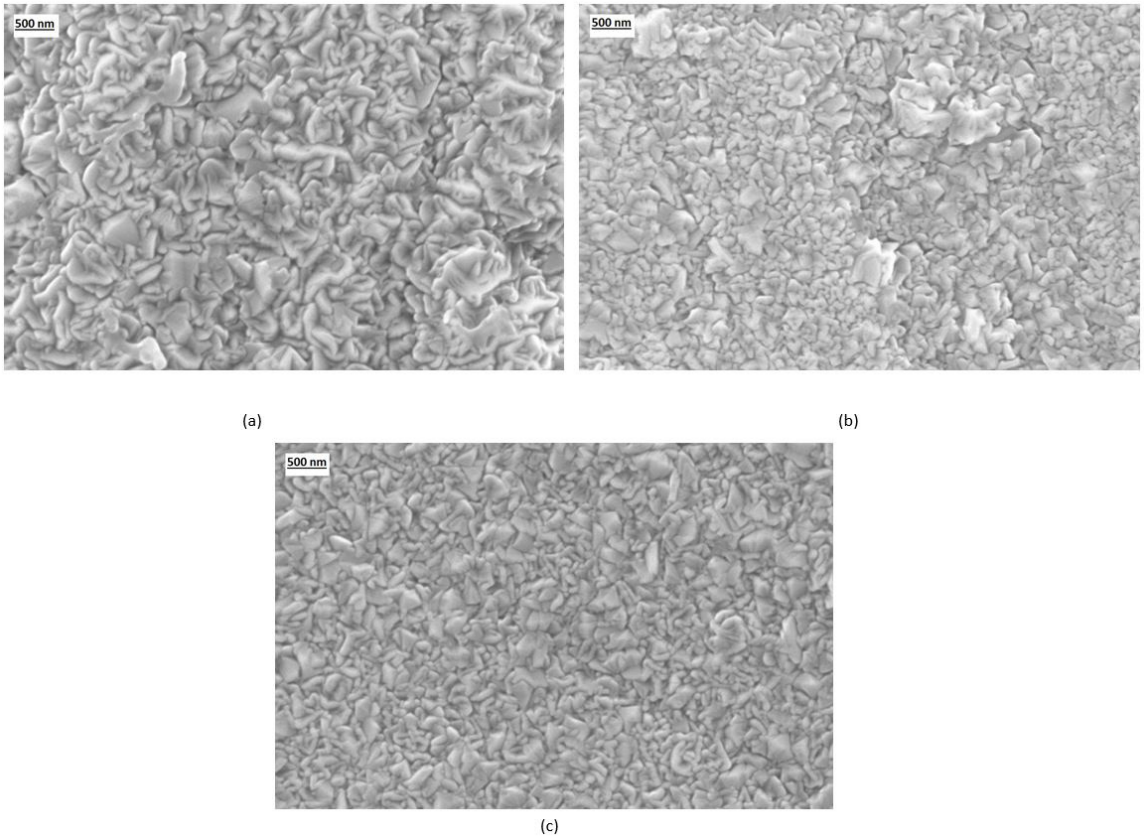

Figure 3. Morphology of AZO coatings prepared at (a) 33%, (b) 43%, and (c) 50% argon partial pressure.

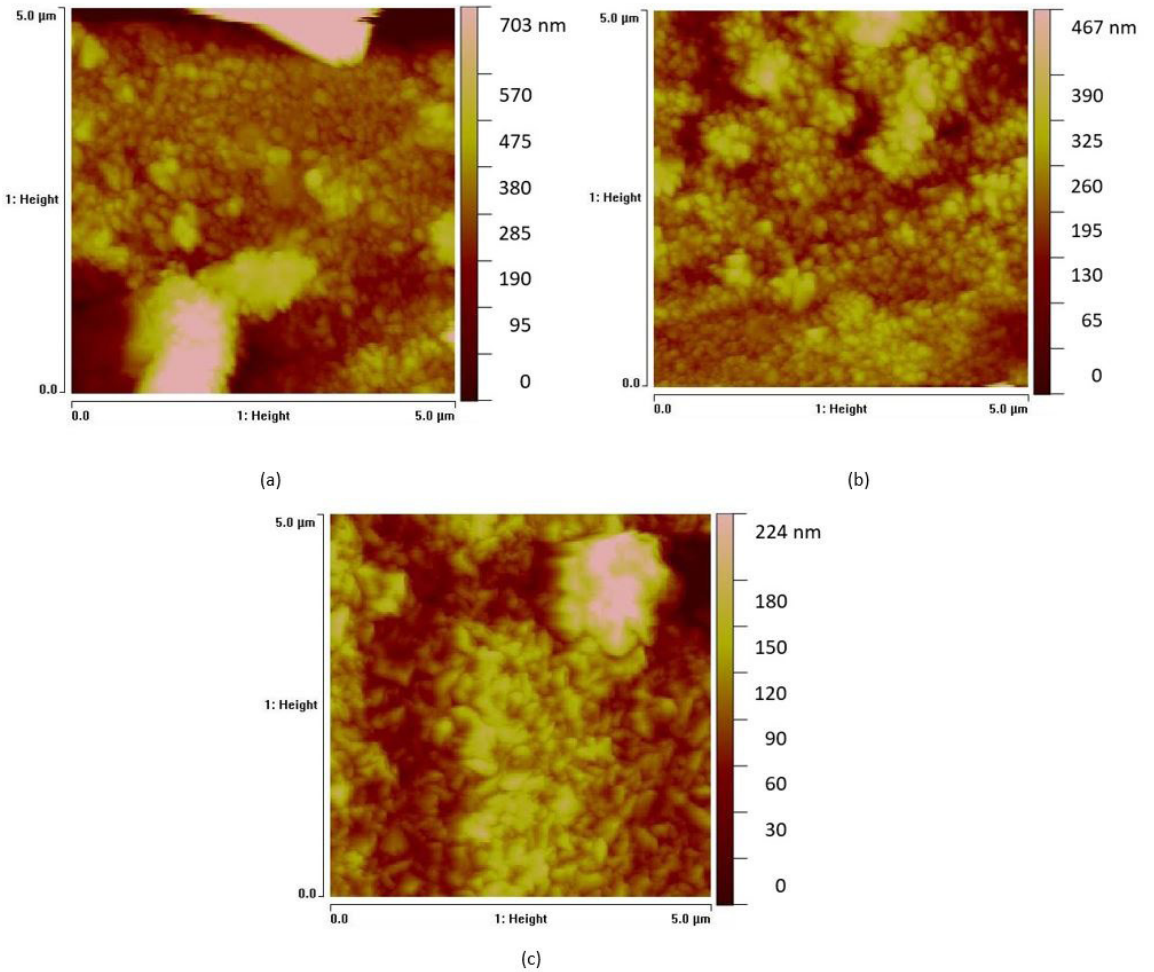

Figure 4. Topography of AZO coatings prepared at (a) 33%, (b) 43%, and (c) 50% argon partial pressure.

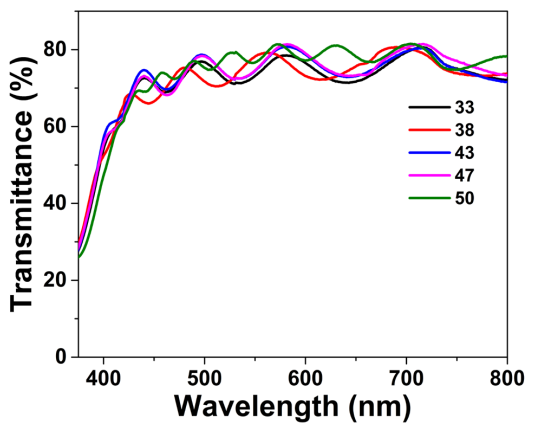

Figure 5. Transmittance spectra of AZO coatings prepared at different argon partial pressures.

diminished when the pressure was reduced from 2.5 Pa to 0.5 Pa. Valenzuela et al.[26] noticed a similar trend and reported that the optical transmittance improved and the electrical characteristics deteriorated with a rise in argon flow rate but without oxygen addition. Tseng et al.[30] also observed 80% transmittance at 193 sccm argon flow rate which decreased at the argon flow rate was reduced to 33 sccm.

The refractive index of the aforementioned coatings was studied using the below Equation 2[31]:

$$\text{Refractive index } n = \left[N + \left(N^2 - n_0^2 n_1^2 \right)^{1/2} \right]^{1/2} \quad (2)$$

where

$$N = \frac{n_0^2 + n_1^2}{2} + 2 n_0 n_1 \frac{T_{max} - T_{min}}{T_{max} T_{min}}$$

n_0 and n_1 represent the refractive index of air and substrate respectively.

The refractive index of AZO coatings developed at 33 to 50% was between 1.53 to 1.50 respectively. Misra et al.[32] and Patel and Rawal[33] examined and concluded that AZO coatings had a constant refractive index.

Calculation of the thickness of the thin films were done using the following Equation 3[31]:

$$t = \frac{M\lambda_1\lambda_2}{2\left[n(\lambda_1)\lambda_2 - n(\lambda_2)\lambda_1\right]} \quad (3)$$

where λ1, n(λ1), λ2 and n(λ2) are corresponding wavelength and index of refraction and M is the number of oscillations.

The thickness of the synthesized coatings studied using the equation showed that with a rise in argon partial pressure the thickness of the developed coatings decreases. The thickness of the developed coatings at 33, 38, 43, 47, and 50% argon partial pressure were 1312, 1138, 1135, 1114, and 1109 nm respectively.

Tauc relation (4) was used to calculate the band gap energy for the aforementioned coatings[34]:

$$\alpha = A\left(h\upsilon - E_g\right)^n / h\upsilon \quad (4)$$

where, $h\upsilon$ is energy of proton energy, n indicated the transition index, and A is a constant.

While the bonding state and atomic composition in the coatings play an important role, defects and impurities also have an impact on the band gap's value. The band gap of the prepared coatings reduced as the argon partial pressure reduced and it can be observed in Figure 6. The band gap energy of the prepared coatings was 2.98 to 3.15 eV for partial pressure of 33 to 50% respectively. Barasategui et al.[29] observed similar results in their research, the band gap energy increased from 3.51 to 3.7 eV with rising argon pressure.

The wettability and surface roughness of the developed Al-doped zinc oxide coatings are illustrated in Figure 7. It was visible from the graphs that the roughness of the surface and hydrophobicity of the coatings decreased as the argon partial pressure increased. An appropriate surface texture must be developed in order to produce hydrophobicity or hydrophilicity. Increases in surface micro and nano-texture cause the contact angle to increase, while it decreases with the decrease in surface roughness. It was clearly observed that the contact angle has a direct correlation with the surface roughness of the thin films and it can be understood by the model proposed by Wenzel (Equation 5)[35]:

$$\cos\theta_w = A\cos\theta \quad (5)$$

where θ indicates WCA on the basis of interfacial energy at the point of the contact angle between three phases and θ_w indicates WCA with rough surface, A signifies the roughness factor which can be defined by the ratio between actual and perceived surface areas which is greater than 1[36].

The coatings prepared at 33% argon exhibited a maximum contact angle of 127.5° and roughness of 703 nm, which decreased to 115.9°, 111.4°, and 105.3° at 38, 43, and 47% argon partial pressure, respectively. At 50% argon, the surface roughness was decreased to 224 nm and likewise the hydrophobicity also decreased to 102°. The roughness of the surface had a positive effect on the wettability properties of the thin films, which was consistent with the research reported elsewhere[37].

The icing characteristics of thin films synthesized under various partial pressures were studied using a Peltier-cooling device at -15 °C. When the thin film icing properties were compared to uncoated samples, it was discovered that ice formation on coated samples was decelerated. The increase in icing time delay on thin films formed at varied partial pressure is seen in Table 2.

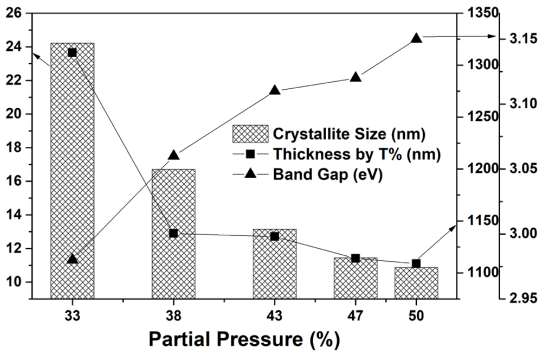

Figure 6. Thickness, Crystallite Size, and Band gap energy of AZO coatings prepared at different argon partial pressures.

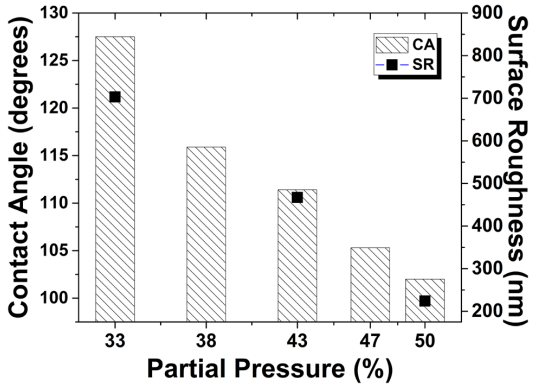

Figure 7. Wettability and surface roughness of AZO coatings prepared at different argon partial pressures.

Coated samples were found to be more stable than uncoated samples in terms of their ability to freeze. It can be seen in Table 2 that when the partial pressure was minimum the time taken for ice formation on the substrate increased by 4.5 folds. Various research has identified a correlation between anti-icing and water hydrophobicity[38,39]. Using materials that have relatively lower surface energy is crucial for developing hydrophobic and anti-icing properties, along with the surface roughness, which is another crucial property for improving the WCA on substrates, which eventually improves the anti-icing properties of the coatings.

The effects of hydrophobicity on ice formation and adhesion were studied by Noormohammed and Sarkar[40]. They concluded that by adjusting the geometry and chemical state, ice-resistant surfaces might be developed. In addition, they found that the adhesion strength of ice reduced as the hydrophobicity of the thin films increased. Multiple studies also demonstrated the importance of high surface roughness and low surface energy in order to increase the contact angle, which in turn enhanced the anti-icing properties. Liu et al.[1] formed ZnO coatings on Al alloy using the sputtering process and analysed how their wettability characteristics changed as a

Table 2. Contact angle and anti-icing characteristics of prepared coatings.

Sputtering Condition	33%	38%	43%	47%	50%
WCA (°)	127.5	115.9	111.4	105.3	102
Time Delay (times/folds)	4.5 x	4.25 x	3.66 x	3.33 x	2.56 x

Table 3. Nomenclatures and Abbreviations.

Nomenclatures and Abbreviations	
°C	Celsius
eV	Electron Volt
Pa	Pascal
°	Degrees
Ω.cm	Ohm centimeter
min.	Minute
θ	Contact angle
sccm	Standard cubic centimeter per minute
mm	Millimeter
µm	Micrometer
nm	Nanometer
W	Watt
Ar	Argon
ZnO	Zinc Oxide
AFM	Atomic Force Microscopy
RF	Radio Frequency
XRD	X-Ray Diffraction
AZO	Aluminum doped Zinc Oxide
TCO	Transparent conducting oxide
FESEM	Field Emission Scanning Electron Microscope
WCA	Water contact angle

function of time. Surfaces developed hydrophobic coatings that delayed the onset of ice. When compared to uncoated substrates, the strength of ice's adherence to coated substrates significantly decreased. Table 3 denotes the nomenclatures and abbreviations used in this paper.

4. Conclusions

Al-doped ZnO coatings were prepared using a variety of argon partial pressure. X-ray diffraction (XRD) revealed that with the rise in partial pressure, the average crystallite size and the intensity of peak (002) decreased. Topography images of the produced coatings showed that the films got smoother from 703 to 224 nm when the partial pressure was increased from 33 to 50%. While the refractive index declined as the argon partial pressure increased, the optical transmittance of the deposited coatings was 82% for 50% and declined to 71% for 33%. The band gap energy of the developed thin films was in the range of 3.51 to 3.7 eV. Data of transmittance was used to calculate an estimate of the film thickness, which ascended from 1109 to 1312 nm when the partial pressure declined. Ice formation was 4.5 times slower on AZO thin films when compared to uncoated substrates when the thin film was developed at 33% argon partial pressure. The deposited thin films were hydrophobic, with a maximum contact angle of 127.5° for 33% partial pressure while the minimum contact angle was 102º for 50% partial pressure. Considering the results of this research, anti-icing applications utilizing hydrophobic surfaces produced using low surface energy materials and specialized textures are promising areas of research. The work described here can serve as a guide for engineers developing anti-icing surfaces for aircraft windshields.

5. Acknowledgements

We appreciate the support of President and Provost of Charotar University of Science and Technology for this research project. We are grateful to IIT Bombay's FIST (Physics) - IRCC SPM Central Facility for allowing us to conduct structural analysis in their lab.

6. References

1. Liu G, Yuan Y, Jiang Z, Youdong J, Liang W. Anti-frosting/anti-icing property of nano-ZnO superhydrophobic surface on Al alloy prepared by radio frequency magnetron sputtering. Mater Res Express. 2020;7(2):026401.
2. Tarquini S, Antonini C, Amirfazli A, Marengo M, Palacios J. Investigation of ice shedding properties of superhydrophobic coatings on helicopter blades. Cold Reg Sci Technol. 2014;100:50-8.
3. Homola MC, Virk MS, Nicklasson PJ, Sundsbø PA. Performance losses due to ice accretion for a 5 MW wind turbine. Wind Energy. 2012;15(3):379-89.
4. Jiang X, Wang S, Zhang Z, Xie S, Wang Y. Study on AC flashover performance and discharge process of polluted and iced IEC standard suspension insulator string. IEEE Trans Power Deliv. 2007;22(1):472-80.
5. Péter Z, Farzaneh M, Kiss LI. Assessment of the current intensity for preventing ice accretion on overhead conductors. IEEE Trans Power Deliv. 2007;22(1):565-74.
6. Chen Y, Chen S, Yu F, Sun W, Zhu H, Yin Y. Fabrication and anti-corrosion property of superhydrophobic hybrid film on copper surface and its formation mechanism. Surf Interface Anal. 2009;41(11):872-7.
7. Chen X, Ma R, Zhou H, Zhou X, Che L, Yao S, et al. Activating the microscale edge effect in a hierarchical surface for frosting suppression and defrosting promotion. Sci Rep. 2013;3(1):1-8.
8. Farhadi S, Farzaneh M, Kulinich SA. Anti-icing performance of superhydrophobic surfaces. Appl Surf Sci. 2011;257(14):6264-9.
9. Bai ZG, Zhang B. Fabrication of a mechanically-stable anti-icing graphene oxide-diatomaceous earth/epoxy coating. Mater Res Express. 2019;6(8):085090.
10. Rawal SK, Chawla AK, Jayaganthan R, Chandra R. Structural, wettability and optical investigation of titanium oxynitride coatings: effect of various sputtering parameters. J Mater Sci Technol. 2012;28(6):512-23.
11. Zheng S, Bellido-Aguilar DA, Wu X, Zhan X, Huang Y, Zeng X, et al. Durable waterborne hydrophobic bio-epoxy coating with improved anti-icing and self-cleaning performance. ACS Sustain Chem& Eng. 2019;7(1):641-9.
12. Zhu Q, Hui M, Jin P, Joo J, Lee C, Le K, et al. Recent advances in nanotechnology-based functional coatings for the built environment. Mater Today Adv. 2022;15:100270.
13. De Oliveira RS, Folli HA, Stegemann C, Horta IM, Damasceno BS, Miyakawa W, et al. Structural, morphological, vibrational and optical properties of GaN films grown by reactive sputtering: the effect of RF power at low working pressure limit. Mater Res. 2022;25:25.

14. Akmal M, Hatta M, Warikh M, Rashid A, Azlan UAH, Azmi A, et al. Influence of yttrium dopant on the structure and electrical conductivity of potassium sodium niobate thin films. Mater Res. 2016;19(6):1-6.
15. Sayed FN, Sreedhara MB, Soni A, Bhat U, Datta R, Bhattacharyya AJ, et al. Li and Na-ion diffusion and intercalation characteristics in vertically aligned TiS_2 nanowall network grown using atomic layer deposition. Mater Res Express. 2019;6:115549.
16. Oliveira LPG, Ribeiro RP, Bortoleto JRR, Cruz NC, Rangel EC. SiOxCyHz-TiO_2 nanocomposite films prepared by a novel PECVD-sputtering process. Mater Res. 2021;24(Suppl. 1):1-9.
17. Li J, Lei L, Li L, Deng B, Zhao G, Jin L, et al. Microstructural evolution and its influence on oxygen diffusion in yttrium-doped ceria thin films. Mater Res Express. 2022;9(4):046404.
18. Bonilha MM, Santos DI, Mohallem NDS, Seara LM, Yonamine AH. Structural, atomic and electrostatic force microscopy analyses on YBCO/PBCO/LCMO superlattices. Mater Res. 2017;20(4):904-11. http://dx.doi.org/10.1590/1980-5373-mr-2016-0725.
19. Patel NP, Chauhan KV. Structural, optical and electrical study of ZnO:Al thin films: a review. Mater Today Proc. 2022;62(6):3386-96.
20. Bussell BC, Gibson PN, Lawton J, Couture P, Sharpe MK, England J, et al. The effect of RF plasma power on remote plasma sputtered AZO thin films. Surf Coat Tech. 2022;442:128402.
21. Wu HW, Chu CH, Chen YF, Chen YW, Tsai WH, Huang SH, et al. Study of AZO thin films under different Ar flow and sputtering power by rf magnetron sputtering. Lect Notes Eng Comput Sci. 2013;2203:790-3.
22. Liu C, He F, Yan N, Zang S, Zuo Y, Ma J. Influence of deposition pressure on properties of ZnO: al films fabricated by RF magnetron sputtering. J Wuhan Univ Technol Mater Sci Ed. 2016;31(6):1235-9.
23. Shain FL, Mani AM, Li LM, Shuib UF, Salleh S, Alias A, et al. Pressure dependence of AZO film deposited by RF powered magnetron sputtering system. Adv Mat Res. 2015;1119:29-33.
24. Han SI, Kim HB. A study on properties of RF-sputtered Al-doped ZnO thin films prepared with different ar gas flow rates. Appl Sci Converg Technol. 2016;25(6):145-8.
25. Gao K, Shen H, Wei Q, Liu Y, Ahmad I. Reduced thermal effect of AZO / Cu / AZO infrared filter film for solar cell. Opt Mater. 2020;110:110534.
26. García-Valenzuela JA, Cabrera-German D, Cota-Leal M, Suárez-Campos G, Martínez-Gil M, Romo-García F, et al. Modulation of argon pressure as an option to control transmittance and resistivity of ZnO:Al films deposited by DC magnetron sputtering: on the dark yellow films at 10 -7 Torr base pressures. Rev Mex Fis. 2018;64(6):566-76.
27. Alghtani AH, Alsharef M, El-Aziz KA. Characterization of iron powder produced by reduction of hot-rolled mill scale in hydrogen gas. Mater Res. 2022;25:e20210575.
28. Wang X, Lei Q, Yuan J, Zhou W, Yu J. Influence of argon gas pressure on the ZnO:AL films deposited on flexible TPT substrates at room temperature by magnetron sputtering. J Wuhan Univ Technol Mater Sci Ed. 2011;26(1):52-5.
29. Barasategui E, Zubizarreta C, Bayón R, Barriga J, Barros R, Martins R, et al. Study of the optical, electrical and corrosion resistance properties of AZO layers deposited by DC pulsed magnetron sputtering. Surf Coat Tech. 2014;271:141-7.
30. Tseng CH, Wang WH, Chang HC, Chou CP, Hsu CY. Effects of sputtering pressure and Al buffer layer thickness on properties of AZO films grown by rf magnetron sputtering. Vacuum. 2010;85(2):263-7.
31. Hasaneen MF, Alrowaili ZA, Mohamed WS. Structure and optical properties of polycrystalline ZnSe thin films: validity of Swanepol's approach for calculating the optical parameters. Mater Res Express. 2020;7(1):016422.
32. Misra P, Ganeshan V, Agrawal N. Low temperature deposition of highly transparent and conducting Al-doped ZnO fi lms by RF magnetron sputtering. J Alloys Compd. 2017;725:60-8.
33. Patel KH, Rawal SK. Influence of power and temperature on properties of sputtered AZO films. Thin Solid Films. 2016;620:182-7.
34. Sparvoli M, Mansano RD, Chubaci JFD. Study of indium nitride and indium oxynitride band Gaps. Mater Res. 2013;16(4):850-2.
35. Lu L, Yao W, Xie Y, Li K, Wan Z. Study on the wettability of biomimetic stainless-steel surfaces inspired by *Bauhinia Linn.* leaf. Surf Coat Tech. 2021;405:126721.
36. Rawal SK, Chawla AK, Chawla V, Jayaganthan R, Chandra R. Structural, optical and hydrophobic properties of sputter deposited zirconium oxynitride films. Mater Sci Eng B. 2010;172(3):259-66.
37. Patel NP, Chauhan KV. Effect of sputtering power and substrate temperature on structural, optical, wettability and anti-icing characteristics of aluminium doped zinc oxide. Mater Res Express. 2022;9(7):076402.
38. Saleema N, Farzaneh M, Paynter RW, Sarkar DK. Prevention of ice accretion on aluminum surfaces by enhancing their hydrophobic properties. J Adhes Sci Technol. 2011;25(1-3):27-40.
39. Wu X, Silberschmidt VV, Hu Z-T, Chen Z. When superhydrophobic coatings are icephobic: role of surface topology. Surf Coat Tech. 2019;358:207-14.
40. Noormohammed S, Sarkar DK. Rf-sputtered Teflon-modified superhydrophobic nanostructured titanium dioxide coating on aluminum alloy for icephobic applications. Coatings. 2021;11(4):432.